AGU PUBLICATIONS

Geophysical Research Letters

RESEARCH LETTER
10.1002/2016GL071755

Key Points:
- The rate constant for the recombination of CaO^+ ions with electrons, which is important in the lower thermosphere, has been measured
- The eightfold larger ratio of Ca^+/Fe^+ ions compared with Ca/Fe atoms between 90 and 100 km can now be explained
- Ca^+ ions in a descending sporadic *E* layer neutralize sufficiently rapidly to explain the sudden growth of sporadic neutral Ca layers

Supporting Information:
- Supporting Information S1

Correspondence to:
J. M. C. Plane,
j.mc.plane@leeds.ac.uk

Citation:
Bones, D. L., M. Gerding, J. Höffner, J. C. G. Martín, and J. M. C. Plane (2016), A study of the dissociative recombination of CaO^+ with electrons: Implications for Ca chemistry in the upper atmosphere, *Geophys. Res. Lett.*, *43*, 12,333–12,339, doi:10.1002/2016GL071755.

Received 27 OCT 2016
Accepted 8 DEC 2016
Accepted article online 12 DEC 2016
Published online 29 DEC 2016

A study of the dissociative recombination of CaO^+ with electrons: Implications for Ca chemistry in the upper atmosphere

D. L. Bones[1], M. Gerding[2], J. Höffner[2], Juan Carlos Gómez Martín[1], and J. M. C. Plane[1]

[1]School of Chemistry, University of Leeds, Leeds, UK, [2]Leibniz Institute of Atmospheric Physics, Rostock University, Kühlungsborn, Germany

Abstract The dissociative recombination of CaO^+ ions with electrons has been studied in a flowing afterglow reactor. CaO^+ was generated by the pulsed laser ablation of a Ca target, followed by entrainment in an Ar^+ ion/electron plasma. A kinetic model describing the gas-phase chemistry and diffusion to the reactor walls was fitted to the experimental data, yielding a rate coefficient of $(3.0 \pm 1.0) \times 10^{-7}$ cm^3 molecule^{-1} s^{-1} at 295 K. This result has two atmospheric implications. First, the surprising observation that the Ca^+/Fe^+ ratio is ~8 times larger than Ca/Fe between 90 and 100 km in the atmosphere can now be explained quantitatively by the known ion-molecule chemistry of these two metals. Second, the rate of neutralization of Ca^+ ions in a descending sporadic *E* layer is fast enough to explain the often explosive growth of sporadic neutral Ca layers.

1. Introduction

Meteoric ablation is the source of metals such as calcium, sodium, and iron in the mesosphere and lower thermosphere (MLT) [*Plane et al.*, 2015]. These metals occur as neutral atoms in layers between 80 and 100 km and atomic ions which become dominant above 95 km. Lidar observations of the neutral metal layers have shown that Ca is significantly depleted with respect to Na and Fe: the Ca/Na and Ca/Fe column abundance ratios are ~0.01 and 0.004 [*Plane et al.*, 2015], compared to their chondritic ratios (in CI type carbonaceous chondrites) of 1.05 and 0.069, respectively [*Asplund et al.*, 2009]. The most likely reason for this depletion is differential ablation, where the highly refractory Ca only ablates from meteoroids which reach temperatures above 2200 K, compared to the relatively volatile elements Na and Fe which largely ablate below 2000 K [*Carrillo-Sanchez et al.*, 2015]. However, in contrast to the neutral ratios, the observed atmospheric Ca^+/Na^+ and Ca^+/Fe^+ ratios are ~0.4 and 0.03 [*Kopp*, 1997], which are much closer to their respective CI ratios.

This result implies that there are important differences in the ion-molecule chemistries of these metals. In this paper we focus on calcium and iron chemistries, because Ca^+ and Fe^+ are chemically reactive ions and therefore behave more alike, compared with the chemically inert Na^+ ion. In the MLT, these ions are largely produced by charge transfer reactions with NO^+ and, to a lesser extent, O_2^+ (photoionization is a much less important ionization process [*Plane et al.*, 2015]). For example [*Rutherford et al.*, 1972],

(R1) $$Ca + NO^+ \rightarrow Ca^+ + NO$$

Above 110 km, the slow dielectronic/radiative recombination of the metallic ions with electrons becomes the dominant neutralization pathway [*Bones et al.*, 2016]. However, between 90 and 100 km the dominant pathway is reaction with O_3 to produce the metal oxide ion [*Broadley et al.*, 2007],

(R2) $$Ca^+ + O_3 \rightarrow CaO^+ + O_2$$

followed by dissociative recombination (DR) with electrons

(R3) $$CaO^+ + e^- \rightarrow Ca + O$$

Since DR reactions generally have rate coefficients $>10^{-7}$ cm^3 molecule^{-1} s^{-1} [*Florescu-Mitchell and Mitchell*, 2006], if reactions (R2) and (R3) were the only chemistry occurring, the lifetime of Ca^+ would be ~10 s, with consequently much lower concentrations than measured by lidar [*Gerding et al.*, 2000; *Granier et al.*, 1985; *Raizada et al.*, 2011] and rocket-borne mass spectrometry [*Kopp*, 1997]. In fact, the reaction of CaO^+ with atomic O

(R4) $$CaO^+ + O \rightarrow Ca^+ + O_2$$

converts the metal oxide ion back to the atomic ion, thus slowing the overall rate of neutralization [*Broadley and Plane*, 2010]. The rate coefficients k_1 [*Rutherford et al*., 1972], k_2 [*Broadley et al*., 2007], and k_4 [*Broadley and Plane*, 2010] have been measured previously, as have the rate coefficients for the analogous reactions of Fe [*Rollason and Plane*, 1998; *Rutherford and Vroom*, 1972; *Woodcock et al*., 2006]. We have recently reported the first measurement of the DR of FeO^+ [*Bones et al*., 2016].

The present paper describes a study of reaction (R3), whose rate coefficient does not appear to have been reported previously. We then use the measured value of k_3 to understand why the Ca^+/Fe^+ ratio between 90 and 100 km is nearly an order of magnitude larger than the Ca/Fe ratio. Finally, we examine the role of ion-molecule chemistry in the phenomenon of sporadic Ca layers (Ca_s). These are very thin layers of Ca which appear suddenly, generally at altitudes around 95 km, and can have peak concentrations more than an order of magnitude above the background average Ca atom layer [*Gerding et al*., 2001]. Simultaneous common-volume measurements of Ca and Ca^+ by lidar provide a unique tool for determining whether Ca_s are produced by the neutralization of Ca^+ in descending sporadic *E* layers, as proposed originally to explain sporadic Na layer formation from Na^+ [*Cox and Plane*, 1998].

2. Experimental Technique

The measurements were made in a flowing afterglow system with a pulsed laser source of metallic ions. The system is described in detail elsewhere [*Bones et al*., 2016]. Briefly, the system consists of a stainless steel flow tube connected to a differentially pumped quadrupole mass spectrometer (Hiden HPR60) running in positive ion mode with pulse counting. An Ar^+/electron plasma is generated by flowing He through a microwave discharge cavity (McCarroll cavity, 145 W at 2450 MHz) and then introducing a flow of Ar into the helium/electron plasma, whereupon the charge is transferred to the Ar largely through Penning ionization. The electron density was measured 12.5 cm upstream of the target by a Langmuir probe (Hiden ESPION). All experiments were conducted at pressures of 1 torr and a temperature of 295 K.

CaO^+ ions (and neutral CaO molecules) were introduced into this plasma by the pulsed laser ablation of a solid target. A neodymium: yttrium/aluminum/garnet laser (8 mJ $pulse^{-1}$ at 532 nm, 10 Hz repetition rate) was directed at a sample of Ca metal with a heavily oxidized surface, mounted on a rotating rod. Isotopic analyses of the ablated ions showed negligible contamination of the signal by Fe^+ (which is isobaric with CaO^+ at $m/z = 56$). For some experimental runs, the laser pulse was loosely focused on the target to change the ratio of CaO to CaO^+ generated in the ablation pulse.

The *relative* concentration of CaO^+ was measured by the mass spectrometer as a function of flow rate (3–5 slm), which is inversely proportional to the time available for the CaO^+ ions to react with the electrons in the plasma before they enter the mass spectrometer (2.1–3.5 ms, corresponding to flow velocities of 69–113 m s^{-1}). The skimmer cone between the flow tube and the first stage of the mass spectrometer had a 4.0 mm orifice biased at −19 V, and the skimmer cone between the first and second stages of the mass spectrometer had a 1.8 mm orifice biased at −89 V. Each CaO^+ measurement was the sum of the $m/z = 56$ signal from three repeat accumulations of 500 laser shots each. These repeat measurements had an average standard deviation of 15%, although for measurements at low flow velocities the standard deviation could be as high as 30%. During the course of an experiment, over typically 2–3 h, the CaO^+ ablation efficiency varied slowly (usually decreasing), and this was corrected for by taking reference CaO^+ signals periodically (at a median flow velocity of 91 m s^{-1}) and fitting a normalization function.

Materials: He (99.995%, BOC Gases) was purified by passing through a trap of dry molecular sieve (4 Å, 1–2 mm, Alfa Aesar) cooled to 77 K. Ar (99.9999%, BOC Gases) was used without further purification. The calcium shot (Sigma-Aldrich) was at least a decade old and extensively oxidized.

3. Experimental Results

The ablation of the oxidized Ca target produced pulses of CaO^+ and CaO (Figure S1 in the supporting information). The CaO then undergoes charge transfer with Ar^+ ions in the plasma:

(R5) $$CaO + Ar^+ \rightarrow CaO^+ + Ar$$

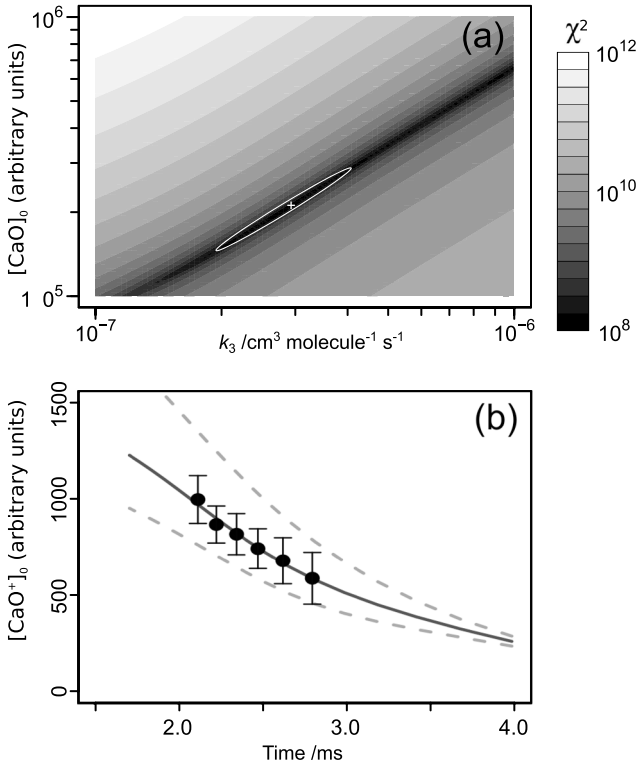

Figure 1. (a) Plot of the χ^2 surface as a function of k_3 and initial neutral CaO concentration produced by pulsed ablation of the Ca target. The white cross indicates the position of the minimum, and the white contour the 1σ envelope of uncertainty. (b) Abundance of CaO^+ as a function of time in the flow tube between the ablation source and detection at the mass spectrometer: measurements (solid circles with 1σ error bars), model fit (solid line), and model run with the upper and lower limits of k_3 (dashed lines).

The upper limit for the rate coefficient k_5 can be calculated from modified Langevin theory [*Su and Chesnavich*, 1982; *Troe*, 1985] to be 8.2×10^{-9} cm^3 molecule^{-1} s^{-1}, using a theoretical dipole moment of 8.8 D and polarizability of 6.6×10^{-24} cm^3 for CaO [*Broadley and Plane*, 2010]. The interactions of CaO^+, CaO, Ar^+, and e^- in the flow tube are then described by the following coupled differential equations:

$$\frac{d[CaO^+]}{dt} = k_5[Ar^+][CaO] - \left(k_{diff}^{CaO^+} + k_3[e^-]\right)\ [CaO^+] \quad \text{(E1)}$$

$$\frac{d[CaO]}{dt} = -\left(k_{diff}^{CaO} + k_5[Ar^+]\right)\ [CaO] \quad \text{(E2)}$$

$$\frac{d[Ar^+]}{dt} = -\left(k_{diff}^{Ar^+} + k_5[CaO]\right)\ [Ar^+] \quad \text{(E3)}$$

$$\frac{d[e^-]}{dt} = -\left(k_{diff}^{e^-} + k_3[CaO^+]\right)\ [e^-] \quad \text{(E4)}$$

The average electron diffusion rate $k_{diff}^{e^-}$ was 948 ± 96 s^{-1} at 1.0 torr. This was determined by measuring the absolute electron density with the Langmuir probe and varying the flow velocity at constant pressure (Figure S2). The electron density immediately after formation of the Ar^+ plasma was then estimated to be $(3.2\pm0.6)\times10^{10}$ cm^{-3}. In the diffusion rate of Ar^+, k_{diff}^{Ar+}, the dominant positive charge carrier was assumed to match the electron diffusion rate under the conditions of ambipolar diffusion which apply because the electrons and ions rapidly equilibrate to the bath gas temperature at the relatively high total pressure of 1 torr [*Smirnov*, 2001]). k_{diff}^{Ca+} was estimated to be 3.7% smaller than k_{diff}^{Ar+} in the bath gas where the Ar/He ratio was 1:10 [*Bones et al.*, 2016]. The diffusion coefficients of neutral CaO are calculated (using the method described in *Self and Plane* [2003]) to be 464 and 95 torr cm^2 s^{-1} in He and Ar, respectively, which corresponds to a wall loss rate k_{diff}^{CaO} of 651 s^{-1}.

Relations (E1)–(E4) were solved numerically to predict the relative CaO^+ concentration at the downstream end of the flow tube. There are two unknowns: k_3 and the initial neutral CaO concentration ($[CaO]_0$). A total of 110 data points were collected in 10 sets of experiments. Each data set was then normalized to the CaO^+ produced by pulsed ablation at the fastest flow velocity, in order to remove the day-to-day variation in the ablation efficiency from the Ca target. The data were then averaged in six reaction time bins with an average bin width of 1.4×10^{-4} s, and a Nelder-Mead iterative simplex algorithm [*Nelder and Mead*, 1965] used to find the best fit of the kinetic model to the six experimental points, by varying k_3 and $[CaO]_0$. The fitting was weighted to the number of data in each time bin, which varied between 10 and 32. Note that in order to model the time-resolved CaO^+ concentration, the model actually requires the product k_5 [CaO] in relations (E1) and (E2); since we fix k_5 to the calculated Langevin limit (see above), $[CaO]_0$ is then the other unknown fitted parameter. Figure 1a is a contour plot of χ^2 as a function of k_3 and $[CaO]_0$, where

$$\chi^2 = \sum_{i=1}^{N}\left(\frac{\left(CaO^+_{expt,i} - CaO^+_{model,i}\right)}{CaO^+_{expt,i}}\right)^2 \quad \text{(E5)}$$

Table 1. Parameters Used in the Monte Carlo Analyses

Parameter	Typical Value	Uncertainty	Source
CaO^+ ion counts	800	±15%	measured
Electron wall loss	$948\ s^{-1}$	±10%	measured
k_{CT}	$8.2\times10^{-9}\ cm^3\ molecule^{-1}\ s^{-1}$	−30%	estimate
$[CaO]_0/[CaO^+]_0$	17	±50%	estimate
Flow velocity	$80\ m\ s^{-1}$	±2%	measured
Initial electron density	$3.2\times10^{10}\ cm^{-3}$	±20%	measured

The minimum on the χ^2 surface yields $k_3(295\ K) = (3.0 \pm 1.0)\times10^{-7}\ cm^3\ molecule^{-1}\ s^{-1}$, where the uncertainty estimate is discussed below. The corresponding value for $[CaO]_0$ is $1.9\times10^5\ molecule\ cm^{-3}$. The ratio of $[CaO]_0/[CaO^+]_0$ produced directly by ablation is estimated to be 17 ± 5. This ratio decreased by 45% when the ablation laser was loosely focused, as expected because a greater fraction of ions would have been produced.

The uncertainty in k_3 was estimated by using Monte Carlo selection of the theoretically calculated and experimentally measured parameters used in the kinetic model, within their uncertainties listed in Table 1 (assuming a top-hat probability distribution). The model was then rerun to compare with the measurements: if the simplex algorithm found a minimum in the χ^2 surface, and the resulting value of k_3 was within the range of 1×10^{-8}–$1\times10^{-5}\ cm^3\ molecule^{-1}\ s^{-1}$ expected for a DR reaction [*Florescu-Mitchell and Mitchell*, 2006], then the value of k_3 was accepted. The mean and standard deviation of k_3 from 2500 model fits then provided the final value of k_3 and the estimate of its uncertainty. Although the determination of k_3 is sensitive to the flow velocity and electron diffusional wall loss, these parameters are measured with high precision. In contrast, k_3 is much less sensitive to the estimated $[CaO^+]_0/[CaO]_0$ ratio and estimate of k_5 using Langevin theory, but these parameters have a greater assigned uncertainty (Table 1) and so make a similar contribution to the overall uncertainty of k_3 (see the supporting information for further details). The white contour line in Figure 1a depicts the envelope of uncertainty around the minimum, which is 44% below the contour line. Figure 1b shows a plot of the measured abundance of CaO^+ (with $\pm1\sigma$ standard deviation) as a function of reaction time. The black line is the model fit through the measured data. The dashed lines show the model output with the upper and lower bounds of k_3. Note that the overall uncertainty is larger than the uncertainty of the measurements because the Monte Carlo analysis included additional uncertainties (Table 1) when determining the uncertainty of k_3.

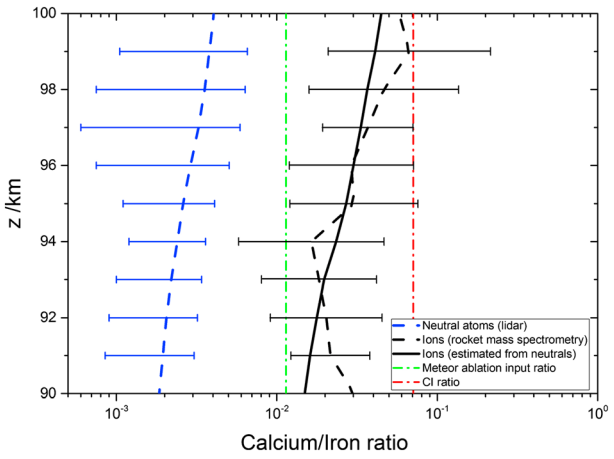

Figure 2. Vertical profiles (90–100 km) of the measured Ca^+/Fe^+ ratio from a series of middle- and high-latitude rocket flights (dashed black line), and the Ca/Fe ratio measured by lidar at 54°N (dashed blue line), from which the Ca^+/Fe^+ ratio is estimated by assuming chemical steady state (black solid line). The CI ratio of the metals (red dashed line) and the modeled meteor ablation ratio (green dashed line) are shown for comparison.

4. Atmospheric Implications

4.1. The Background Ca^+ Concentration in the Lower Thermosphere

In order to study the ion-molecule chemistry of calcium in the MLT, we assign a $T^{-0.5}$ temperature dependence to k_3, which is typical for DR reactions [*Florescu-Mitchell and Mitchell*, 2006]. Reaction (R3) is 45% slower than the DR reaction of FeO^+ at room temperature [*Bones et al.*, 2016]. We now examine the consequences of this for explaining the very different Ca/Fe and Ca^+/Fe^+ ratios in the 90–100 km region of the atmosphere.

Figure 2 illustrates the problem. The dashed black line shows the $[Ca^+]/[Fe^+]$ ratio profile measured by rocket-borne mass spectrometry. The mean and

Table 2. Rate Coefficients Required to Estimate $[Ca^+]/[Fe^+]$ From [Ca]/[Fe]

Reaction	k (200 K) cm^3 $molecule^{-1}$ s^{-1}	Source
$Ca + NO^+ \rightarrow Ca^+ + NO$	4.0×10^{-9}	*Rutherford et al.* [1972]
$Fe + NO^+ \rightarrow Fe^+ + NO$	9.2×10^{-10}	*Rutherford and Vroom* [1972]
$Ca^+ + O_3 \rightarrow CaO^+ + O_2$	3.9×10^{-10}	*Broadley et al.* [2007]
$Fe^+ + O_3 \rightarrow FeO^+ + O_2$	3.7×10^{-10}	*Rollason and Plane* [1998]
$CaO^+ + O \rightarrow Ca^+ + O_2$	4.2×10^{-11}	*Broadley et al.* [2008]
$FeO^+ + O \rightarrow Fe^+ + O_2$	3.0×10^{-11}	*Woodcock et al.* [2006]
$CaO^+ + e^- \rightarrow Ca + O$	3.7×10^{-7}	This study
$FeO^+ + e^- \rightarrow Fe + O$	6.7×10^{-7}	*Bones et al.* [2016]

standard deviation were calculated from seven flights covering a range of latitudes and local times (note that the *geometric*, rather than arithmetic, mean is used because of the small data set; the geometric mean is defined as $\overline{x} = \sqrt[n]{x_1 x_2 \cdots x_n}$). Details of the flights are listed in the supporting information. The dashed blue line shows the mean [Ca]/[Fe] ratio computed from simultaneous and common volume lidar measurements of Ca and Fe at Kühlungsborn, Germany (54°N). Data from 22 nights (each with 2–9 h of measurements) were used; the total data set is ~120 h of measurements. The measurements were performed between April 1997 and March 1999. The standard deviation was calculated from the mean ratio of each night.

These two profiles should be compared with the chondritic CI ratio (red dashed line) [*Asplund et al.*, 2009], and the ratio of the meteoric ablation fluxes of Ca and Fe, calculated by applying the chemical ablation model to an astronomical model of cosmic dust [*Carrillo-Sanchez et al.*, 2015]. Note that the ablation ratio is a factor of 7 times smaller than the CI ratio because of the differential ablation of the two elements. The $[Ca^+]/[Fe^+]$ ratio falls between the CI and the ablation ratios, and the [Ca]/[Fe] ratio is significantly below even the ablation ratio.

Since the rates of reactions (R1)–(R4) in the MLT are reasonably fast between 90 and 100 km, and the dominant forms of these metals in this region of the atmosphere are neutral and ionized atoms [*Plane et al.*, 2015], the kinetic steady state approximation can be applied to Ca^+ and CaO^+:

$$\frac{d[Ca^+]}{dt} = k_1[NO^+][Ca] - k_2[O_3][Ca^+] + k_4[O][CaO^+] \approx 0 \quad \text{(E6)}$$

$$\frac{d[CaO^+]}{dt} = k_2[O_3][Ca^+] - k_3[e^-][CaO^+] - k_4[O][CaO^+] \approx 0 \quad \text{(E7)}$$

Hence,

$$\frac{[Ca^+]}{[Ca]} = k_1[NO^+]\frac{(k_3[e^-] + k_4[O])}{k_2 k_3[O_3][e^-]} \quad \text{(E8)}$$

Since $k_4[O]$ is generally more than 3 orders of magnitude larger than k_3 $[e^-]$ between 90 and 100 km [*Plane et al.*, 2015],

$$\frac{[Ca^+]}{[Ca]} \approx k_1[NO^+]\frac{k_4[O]}{k_2 k_3[O_3][e^-]} \quad \text{(E9)}$$

Dividing equation (E9) by the analogous equation for $[Fe^+]/[Fe]$, the atmospheric constituents $[NO^+]$, $[O_3]$, [O], and $[e^-]$ cancel. Rearranging, and using the rate coefficients listed in Table 2, $[Ca^+]/[Fe^+] = 8.3[Ca]/[Fe]$. When the lidar measurement of the [Ca]/[Fe] ratio is multiplied by this factor, the estimated $[Ca^+]/[Fe^+]$ ratio (solid black line in Figure 2) is seen to be in good agreement with the ion ratio measured by mass spectrometry. Inspection of Table 2 shows that there are two reasons for this large increase in the ratio of the ions compared with the neutrals. First, charge transfer between NO^+ and Ca is ~5 times faster than for Fe. Second, the DR of CaO^+ is ~50% slower than FeO^+.

4.2. Sporadic Ca Layers

We now examine whether the mechanism for sporadic metal layer formation in a descending sporadic *E* layer [*Cox and Plane*, 1998] can explain the appearance of Ca_s below 100 km. Figures 3a and 3b show the lidar observations of Ca^+ and Ca on 9 August 1995 at Juliusruh on the island of Rügen, Germany (55°N). In Figure 3a, a pronounced layer of Ca^+ ions, confirmed by ionosonde measurements to be part of a sporadic *E* layer (shown with white crosses in the figure), descends from 100 km to 93 km at a rate of ~4 km h^{-1}.

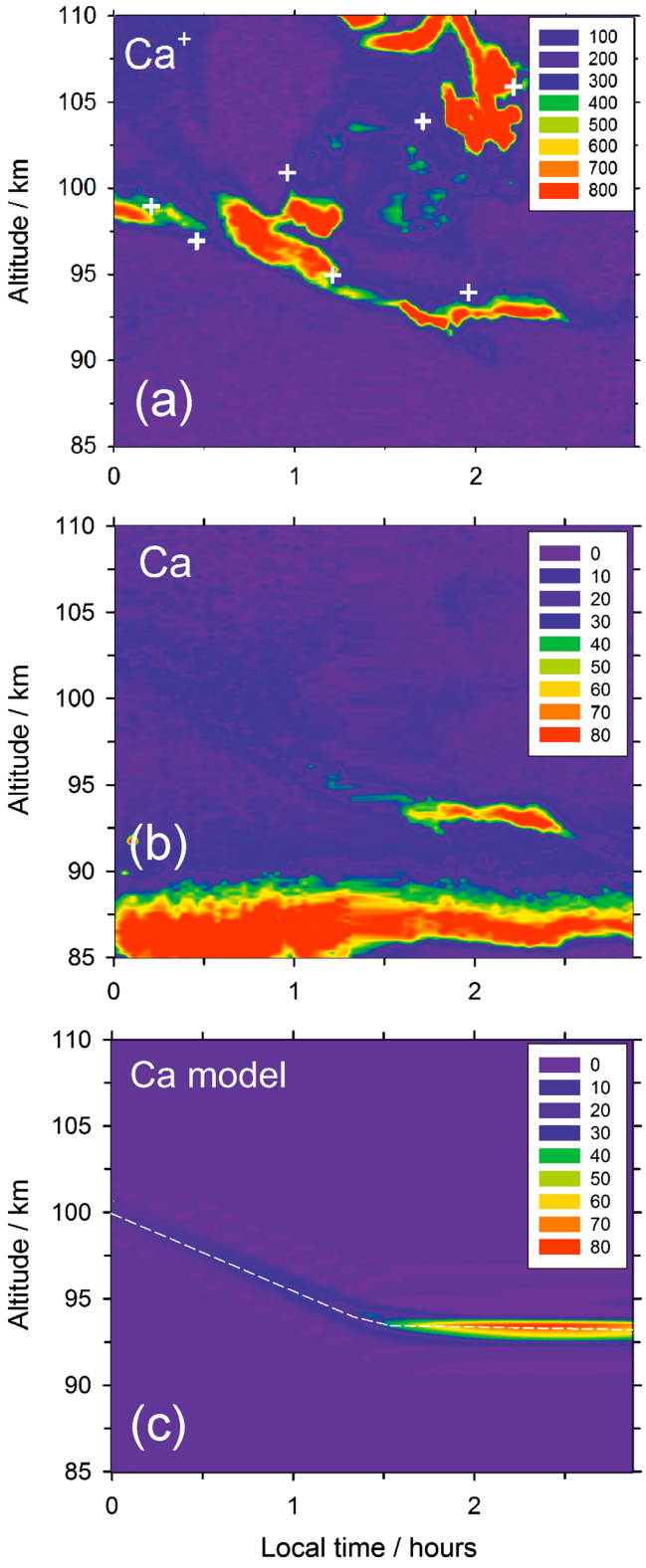

Figure 3. Lidar observations of (a) Ca^+ and (b) Ca on 9 August 1995 at Juliusruh, Germany. The white crosses in Figure 3a indicate the sporadic *E* layer heights measured by ionosonde. (c) Modeled production of Ca from the Ca^+ ions in a sporadic *E* layer whose descent is indicated by the dashed white line. The Ca/Ca^+ concentration units are atom cm^{-3}.

Figure 3b illustrates the simultaneous neutral Ca measurements, with the background Ca layer continuously present with a peak around 87 km. Note that a Ca_s layer appears at 0140 LT once the Ca^+ layer has descended to 94 km. In contrast, the patches of relatively high concentrations of Ca^+ above 95 km that occur around 0100 and 0200 LT are not accompanied by significant concentrations of Ca.

We now use the model of *Cox and Plane* [1998] to simulate the production of Ca in this descending sporadic *E* layer. The sporadic *E* layer is initialized with the measured Ca^+ density of 810 cm^{-3} and Fe^+, Mg^+, Na^+, and Si^+ densities which are scaled to this using their relative abundance factors measured by *Kopp* [1997]. The total metal ion (and hence electron) density at 105 km is then 8.9×10^4 cm^{-3}, consistent with the ionosonde electron density measurements which ranged from (4.5 to 10.5) $\times 10^4$ cm^{-3} between 2300 and 0000 LT. The layer is set to have a full width at half maximum of 1.5 km. Note that the sporadic layer is assumed to have a large horizontal homogeneous extent so that advection does not play a role while the layer is descending.

The ion-molecule chemistry of Ca from the present study and the other four meteoric metals [*Plane et al.*, 2015] are included in the model, along with background atmospheric densities of O_3, O, total density, and temperature from the 1-D general mesospheric model MESOMOD [*Murray and Plane*, 2005]. Figure 3c shows the modeled production of Ca in the descending sporadic *E* layer (the background Ca layer is not modeled in this simulation). The layer, whose position is indicated by the dashed white line, descends at a constant rate to 93 km where the ions are then dumped, as indicated by the Ca^+ observations in Figure 3a. The model successfully reproduces the height and *absolute* concentration of the resulting Ca_s, which is an important test of the reaction kinetics, since inspection of Figure 3 shows that only ~10% of the

available Ca^+ is converted to Ca during the observational period. Moreover, very little neutral Ca is produced until the ion layer descends below 95 km, consistent with Figure 3b, because the rate of neutralization of Ca^+ depends on $[O_3]$ and inversely on [O] (equation (E9)). Since $[O_3]$ increases ~100-fold between 105 and 93 km, and [O] is approximately constant, these ion neutralization rates increase by roughly 2 orders of magnitude. This causes the production of Ca to occur at the dump altitude, but not higher up—so long as the rate of descent of the sporadic *E* layer is sufficiently fast.

5. Conclusions

The rate coefficient for the dissociative recombination of CaO^+ has been measured for the first time and is found to be $(3.0 \pm 1.0) \times 10^{-7}\,cm^3\,molecule^{-1}\,s^{-1}$ at 295 K. This result has two atmospheric implications. First, the surprising observation that the Ca^+/Fe^+ ratio is ~8 times larger than Ca/Fe between 90 and 100 km can now be explained by the known ion-molecule chemistry of these two metals. Second, the rate of neutralization of Ca^+ ions in a descending sporadic *E* layer is fast enough to explain the often explosive growth of sporadic Ca layers.

Acknowledgments
This work was supported by the European Research Council (project 291332-CODITA). The ionosonde data were provided by Jens Mielich (IAP, Kühlungsborn). The mass spectrometric data (provided by E. Kopp, University of Bern) and the experimental data sets are available upon request to J.M.C.P. and the lidar data from J.H.

References

Asplund, M., N. Grevesse, A. J. Sauval, and P. Scott (2009), The chemical composition of the Sun, in *Annual Review Astronomy and Astrophysics*, edited by R. Blandford, J. Kormendy and E. van Dishoeck, pp. 481–522, Annual Reviews, Palo Alto, doi:10.1146/annurev.astro.46.060407.145222.

Bones, D. L., J. M. C. Plane, and W. Feng (2016), Dissociative recombination of FeO^+ with electrons: Implications for plasma layers in the ionosphere, *J. Phys. Chem. A*, *120*, 1369–1376.

Broadley, S. L., and J. M. C. Plane (2010), A kinetic study of reactions of calcium-containing molecules with O and H atoms: Implications for calcium chemistry in the upper atmosphere, *Phys. Chem. Chem. Phys.*, *12*, 9095–9107.

Broadley, S. L., T. Vondrak, and J. M. C. Plane (2007), A kinetic study of the reactions of Ca^+ ions with O_3, O_2, N_2, CO_2 and H_2O, *Phys. Chem. Chem. Phys.*, *9*, 4357–4369.

Broadley, S., T. Vondrak, T. G. Wright, and J. M. C. Plane (2008), A kinetic study of Ca-containing ions reacting with O, O_2, CO_2 and H_2O: Implications for calcium ion chemistry in the upper atmosphere, *Phys. Chem. Chem. Phys.*, *10*, 5287–5298.

Carrillo-Sanchez, J. D., J. M. C. Plane, W. Feng, D. Nesvorny, and D. Janches (2015), On the size and velocity distribution of cosmic dust particles entering the atmosphere, *Geophys. Res. Lett.*, *42*, 6518–6525, doi:10.1002/2015GL065149.

Cox, R. M., and J. M. C. Plane (1998), An ion-molecule mechanism for the formation of neutral sporadic Na layers, *J. Geophys. Res.*, *103*, 6349–6359, doi:10.1029/97JD03376.

Florescu-Mitchell, A. I., and J. B. A. Mitchell (2006), Dissociative recombination, *Phys. Rep. Rev. Phys. Lett.*, *430*, 277–374.

Gerding, M., M. Alpers, U. von Zahn, R. J. Rollason, and J. M. C. Plane (2000), Atmospheric Ca and Ca^+ layers: Midlatitude observations and modeling, *J. Geophys. Res.*, *105*, 27,131–27,146, doi:10.1029/2000JA900088.

Gerding, M., M. Alpers, J. Hoffner, and U. von Zahn (2001), Sporadic Ca and Ca^+ layers at mid-latitudes: Simultaneous observations and implications for their formation, *Ann. Geophys.*, *19*, 47–58.

Granier, C., J. P. Jegou, and G. Megie (1985), Resonant lidar detection of Ca and Ca^+ in the upper atmosphere, *Geophys. Res. Lett.*, *12*, 655–658, doi:10.1029/GL012i010p00655.

Kopp, E. (1997), On the abundance of metal ions in the lower ionosphere, *J. Geophys. Res.*, *102*, 9667–9674, doi:10.1029/97JA00384.

Murray, B. J., and J. M. C. Plane (2005), Modelling the impact of noctilucent cloud formation on atomic oxygen and other minor constituents of the summer mesosphere, *Atmos. Chem. Phys.*, *5*, 1027–1038.

Nelder, J. A., and R. Mead (1965), A simplex method for function minimization, *Comp. J.*, *7*, 308–313.

Plane, J. M. C., W. Feng, and E. C. M. Dawkins (2015), The mesosphere and metals: Chemistry and changes, *Chem. Rev.*, *115*, 4497–4541.

Raizada, S., C. A. Tepley, N. Aponte, and E. Cabassa (2011), Characteristics of neutral calcium and Ca^+ near the mesopause, and their relationship with sporadic ion/electron layers at Arecibo, *Geophys. Res. Lett.*, *38*, L09103, doi:10.1029/2011GL047327.

Rollason, R. J., and J. M. C. Plane (1998), A study of the reactions of Fe^+ with O_3, O_2 and N_2, *J. Chem. Soc. Faraday Trans.*, *94*, 3067–3075.

Rutherford, J. A., and D. A. Vroom (1972), Formation of iron ions by charge transfer, *J. Chem. Phys.*, *57*, 3091–3093.

Rutherford, J. A., B. R. Turner, D. A. Vroom, and R. F. Mathis (1972), Formation of calcium ions by charge transfer, *J. Chem. Phys.*, *57*, 3087–3091.

Self, D. E., and J. M. C. Plane (2003), A kinetic study of the reactions of iron oxides and hydroxides relevant to the chemistry of iron in the upper mesosphere, *Phys. Chem. Chem. Phys.*, *5*, 1407–1418.

Smirnov, B. R. (2001), *Physics of Ionized Gases*, John Wiley, Chichester.

Su, T., and W. J. Chesnavich (1982), Parameterization of the ion-polar molecule collision rate constant by trajectory calculations, *J. Chem. Phys.*, *76*, 5183–5185.

Troe, J. (1985), Statistical adiabatic channel model of ion neutral dipole capture rate constants, *Chem. Phys. Lett.*, *122*, 425–430.

Woodcock, K. R. S., T. Vondrak, S. R. Meech, and J. M. C. Plane (2006), A kinetic study of the reactions $FeO^+ + O$, $Fe^+.N_2 + O$, $Fe^+.O_2 + O$ and $FeO^+ + CO$: implications for sporadic *E* layers in the upper atmosphere, *Phys. Chem. Chem. Phys.*, *8*, 1812–1821.